Adiabatic quantum computing with qubit ensembles

Naeimeh Mohseni,[1,2,3] Marek Narozniak,[4,5] Alexey N. Pyrkov,[6]
Valentin Ivannikov,[4,1] Jonathan P. Dowling,[7] and Tim Byrnes[4,5]

[1] *State Key Laboratory of Precision Spectroscopy, School of Physical and Material Sciences, East China Normal University, Shanghai 200062, China*
[2] *Max-Planck-Institut für die Physik des Lichts, Staudtstrasse 2, 91058 Erlangen, Germany*
[3] *Department of Physics, Institute for Advanced Studies in Basic Sciences(IASBS), Zanjan 45137-66731, Iran*
[4] *New York University Shanghai, 1555 Century Ave, Pudong, Shanghai 200122, China*
[5] *Department of Physics, New York University, New York, NY 10003, USA*
[6] *Institute of Problems of Chemical Physics RAS, Acad. Semenov av., 1, Chernogolovka, 142432, Russia*
[7] *Hearne Institute for Theoretical Physics, Department of Physics and Astronomy, Louisiana State University, Baton Rouge, Louisiana 70803, USA*

(Dated: September 24, 2019)

In the standard approach to adiabatic quantum computing (AQC), quantum information stored on qubits are adiabatically evolved to find the ground state of a problem Hamiltonian. Here we investigate a variation of AQC where qubit ensembles are used in place of qubits. We identify two distinct regimes for a given problem Hamiltonian under this mapping as a function of the ensemble size N. At a critical ensemble size N_c, the nature of the first excited state changes from being macroscopically distinct spin configuration to a single particle perturbation of the ground state. Above N_c the minimum gap for large ensembles is well predicted by mean-field theory and the AQC performance improves with N, realizing error-suppression due to duplication of the quantum information. While below N_c the performance is mixed, and can increase with N. For randomly chosen problem instances Nc tends to be smaller than realistic ensemble sizes, hence we expect the ensemble version of AQC to work well in a great majority of cases. Our approach shows it is possible to perform AQC without the necessity of controlling individual qubits, allowing an alternative route towards implementing AQC.

I. INTRODUCTION

Adiabatic quantum computing (AQC) is an alternative approach to traditional gate-based quantum computing where quantum adiabatic evolution is performed in order to achieve a computation [1–4]. In the scheme, the aim is to find the ground state of a Hamiltonian H_Z which encodes the problem to be solved and can be considered an instance of quantum annealing [5–8]. In addition, an initial Hamiltonian H_X, which does not commute with the problem Hamiltonian, is prepared, such that the ground state is known. For example, a common choice of these Hamiltonians are

$$H_Z^{(\text{qubit})} = \sum_{i=1}^{M}\sum_{j=1}^{M} J_{ij}\sigma_i^z\sigma_j^z + \sum_{i=1}^{M} K_i\sigma_i^z, \tag{1}$$

$$H_X^{(\text{qubit})} = -\sum_{i=1}^{M}\sigma_i^x, \tag{2}$$

where $\sigma_i^{x,z}$ are Pauli matrices on site i, and J_{ij} and K_i are coefficients which determine the problem to be solved, and there are M qubits. The form of (1) as chosen is rather general and can encode a wide variety of optimization problems. For example, MAX-2-SAT and MAXCUT can be directly encoded in (1). As these are NP-complete problems, it then follows that any other NP-complete problem can be mapped to it in polynomial time [9–11]. AQC then proceeds by preparing the initial state of the quantum computer in the ground state of H_X, then applying the time-varying Hamiltonian

$$H = (1-\lambda)H_X + \lambda H_Z, \tag{3}$$

where λ is a time-varying parameter that is swept from 0 to 1. Intense investigation into the performance of AQC has been performed since its original introduction, demonstrating its performance for various problems [12–15] and characterizing the effects of decoherence [16–22].

In the AQC framework, the speed of the computation is given by how fast the adiabatic sweep is performed. To maintain adiabaticity, one must perform the sweep sufficiently slowly, such that the system remains in the ground state throughout the evolution. The sweep time is known to be proportional to the inverse square of the minimum energy gap of the Hamiltonian (3) [2, 13, 15, 23]. One of the attractive features of AQC is that time-sequenced gates do not need to be applied, but it is nevertheless known to be equivalent to gate-based quantum computation [24, 25], with many explicit mappings performed [13, 26]. Numerous experimental demonstrations have been performed both at small [27–31] and larger scale [32–37]. The main outstanding problems for AQC is to fully understand the performance and effectively combat decoherence in AQC such that it can be applied to real-world combinatorial problems [4, 38, 39].

In this paper, we investigate a variant of the AQC Hamiltonians (1) and (2) where ensembles of qubits are used to encode the optimization problem, instead of gen-

uine qubits. Specifically, we study the Hamiltonians

$$H_Z = \frac{1}{N}\sum_{i=1}^{M}\sum_{j=1}^{M} J_{ij} S_i^z S_j^z + \sum_{i=1}^{M} K_i S_i^z \tag{4}$$

$$H_X = -\sum_{i=1}^{M} S_i^x \tag{5}$$

where $S_i^{x,z} = \sum_{n=1}^{N} \sigma_{i,n}^{x,z}$ are total spin operators for an ensemble consisting of N qubits. In this case M is the number of ensembles. Here, $\sigma_{i,n}$ denotes the Pauli operator for the nth qubit within the ith ensemble. The matrices J_{ij} and K_i are the same as that in (1) and we take $J_{ij} = J_{ji}$ and $J_{ii} = 0$. AQC then proceeds in the same way as described in Eq. (3). Each of the ensembles are initially prepared in a fully polarized state of $\langle S_i^x \rangle = N$ and adiabatically evolved to the ground state of H_Z. The aim will be to investigate whether the ensemble version of the Hamiltonian can be used in place of the qubit Hamiltonian, such that the ground state configuration of (1) is found using (4) and (5). We characterize the nature of the ground and excited states of the ensemble Hamiltonian and assess the performance of AQC in comparison to the original qubit problem.

The Hamiltonians (4) and (5) can be considered an error-suppressing encoding of the original AQC Hamiltonians (1) and (2), respectively. The use of an ensemble duplicates the quantum information since the N qubits within an ensemble are in the same state at the start and at the end of the adiabatic evolution. Such error suppression strategies have been investigated before in the context of AQC [40–42]. Jordan, Farhi, and Shor [41] introduced an encoding capable of detecting the presence of single qubit errors, which are suppressed by an additional energy penalty term in the total Hamiltonian. Pudenz, Lidar and co-workers [40], experimentally demonstrated a bit flip code on ensembles of three qubits and showed that errors could be suppressed in an antiferromagnetic chain. Young, Sarovar, and Blume-Kohout [38, 39] showed that such energy penalty approaches could be part of a unified theory with dynamical decoupling, although constructing a genuine error-correction code seems problematic. While these works all show that such error-suppressing strategies are potentially beneficial, the ensemble Hamiltonian (4), and a more detailed investigation on the behavior of the minimum gap and performance for more complex problem instances possessing local minima, has not been performed.

In addition to error-suppression, the ensemble Hamiltonians (4) and (5) are of interest from an experimental perspective, since they offer an alternative way to implement AQC. The Hamiltonian is written completely in terms of the total spin of ensembles of qubits. This means that only global control of *ensembles* of qubits, instead of *individual* qubits, is necessary. This is technically a much easier task, and has been performed in various contexts, particularly with neutral atom ensembles [43–47]. In this study, we do not discuss in detail the implementation of the Hamiltonians (4) and (5) since they can be potentially realized in a variety of systems [40]. Further details of the implementation with neutral atom ensembles on atom chips can be found in Refs. [48, 49] and the Appendix A.

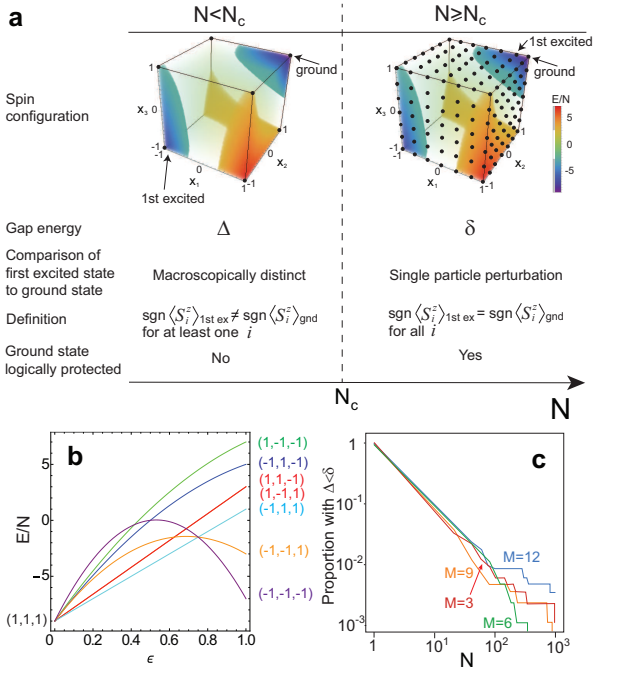

FIG. 1. Properties of the problem Hamiltonian H_Z. (a) Summary of the two regimes for the ensemble version of the problem Hamiltonian H_Z. The cube shows the energy landscape of a typical instance of (4) with rescaled variables $x_i = \langle S_i^z \rangle / N$. Dots indicate allowed states for $N = 1$ (left) and $N = 6$ (right). Only states on the visible faces are shown for clarity. (b) Energy variation for the problem instance as Fig. 1(a) along a linear trajectory from the ground state $x_1 = x_2 = x_3 = 1$ to other hypercube corners specified by $(x_1^{(f)}, x_2^{(f)}, x_3^{(f)})$. The trajectory is defined by $x_i = 1 - (1 - x_i^{(f)})\varepsilon$, where $\varepsilon = 0$ is the ground state and $\varepsilon = 1$ is another hypercube corner. Parameters used are $M = 3$, $J_{12} = -2, J_{13} = -1, J_{23} = -1, K_1 = 1, K_2 = 0, K_3 = -2$. (c) Proportion of 800 randomly generated problem instances with $\Delta < \delta$ (i.e. $N < N_c$) as a function of the ensemble size N.

II. PROPERTIES OF THE PROBLEM HAMILTONIAN H_Z

We first examine the properties of the ensemble version of the (classical) problem Hamiltonian (4). The typical energy landscape of the Hamiltonian H_Z is shown in Fig. 1(a). The axes are plotted with rescaled spin variables $x_i = \langle S_i^z \rangle / N$. For the corners of the hypercube $x_i = \pm 1$, the energy eigenvalues of the ensemble Hamiltonian H_Z reduces to that of the qubit version (1) up to an overall scaling factor of N. This is a general result which

is true by virtue of the structure of the ensemble and qubit problem Hamiltonians H_Z (see Appendix B). The primary difference between (4) and (1) is then that the ensemble version can take a discrete set of intermediate values of x_i between the ± 1 values.

In Fig. 1(b) we show the variation of the energy starting from the ground state to the remaining hypercube corners. The variation always follows a quadratic form with an initially positive slope. This can be shown to be generally true following from the quadratic form of (4) (see Appendix B). This fact can be used to show that for any point along a trajectory connecting the ground state to another hypercube corner has energies greater than the ground state (see Appendix B). From the above structure of the energy landscape, one can deduce that the ground states of the Hamiltonians (1) and (4) have logically equivalent spin configurations. We define the logically equivalent states of the qubit and ensemble systems according to

$$\mathrm{sgn}[\langle \sigma_i^z \rangle^{(\mathrm{qubit})}] = \mathrm{sgn}[\langle S_i^z \rangle^{(\mathrm{ens})}], \tag{6}$$

for all i. This is also known as a majority vote encoding of the ensemble to give the logical state, and has been considered in other error mitigation schemes for AQC [38, 40, 42]. Thus finding the ground state spin configuration of (4) gives the same information as (1).

In AQC, one of the parameters which plays a central role is the gap energy, i.e. the energy between the ground and first excited state. The simple structure of the Hamiltonian (4) allows us to deduce that for a given N, there are two different regimes for the gap energy. For the particular example shown in Fig. 1(a), we see that there are two hypercube corner states $(x_1, x_2, x_3) = (1, 1, 1)$ and $(-1, -1, -1)$ with relatively similar energies of ϵ_0 and ϵ_1, respectively. For the qubit case (1) the difference between the two lowest energy hypercube corners is the gap energy. In the ensemble case, the energy difference between these two hypercube corners is

$$\Delta = N(\epsilon_1 - \epsilon_0), \tag{7}$$

since for extremal values $|x_i| = 1$ the energies are related by a factor of N.

If N is sufficiently small, Δ remains the gap energy for the ensemble case. However, for enough large N this becomes less and less likely, and the first excited state is a single qubit spin flip of the ground state. Specifically, we have the state such that on the kth ensemble $S_k^z = \pm(N-2)$, and the remaining ensembles $S_i^z = \pm N, \forall i \neq k$. The energy gap for this single qubit flip state is

$$\delta = \min_k \left[-2\sigma_k \left(K_k + 2 \sum_j J_{kj} \sigma_j \right) \right], \tag{8}$$

where $\sigma_i = \langle \sigma_i^z \rangle_{\mathrm{gnd}}^{(\mathrm{qubit})} = \mathrm{sgn}(\langle S_i^z \rangle_{\mathrm{gnd}}^{(\mathrm{ens})})$, and expectation values are taken with respect to the ground state. The minimum function picks the smallest value from the range $k \in [1, M]$.

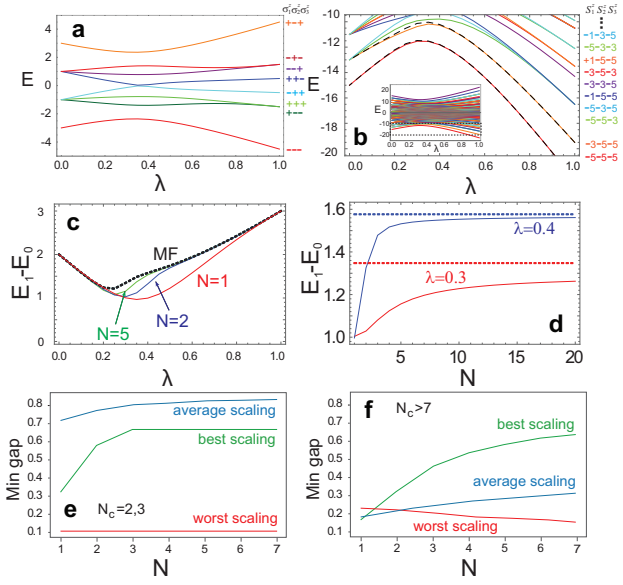

FIG. 2. Energy spectrum and gap energies of the adiabatic quantum computing Hamiltonian. Spectrum of (3) with $M = 3$ with (a) $N = 1$ and (b) $N = 5$ for parameters $J_{12} = -0.5, J_{13} = 0, J_{23} = -1, K_1 = 0.5, K_2 = 0, K_3 = 1$. The mean field approximation for the $N = 5$ is shown as the dashed lines for the ground and first excited state. (c) The gap energy for the ensemble qubit numbers as shown. (d) Scaling of the gap energy with N for two values of λ as shown. The mean field (MF) approximation is shown as the dotted line in (c) and (d). (e) The minimum gap versus N for 60 random instances of problems with $N_c = 2, 3$. The average minimum gap, as well as the largest (best) and smallest (worst) instances are shown. (f) Same as (e) for problems with $N_c > 7$.

Whether Δ or δ is the gap energy depends upon N and the particular parameter choice of J_{ij} and K_i made. As N is increased, at some point there will always be a crossover such that the gap is δ, since (7) is proportional to N while (8) has no dependence on N. Let us call N_c the smallest value of N such that $\Delta > \delta$. For a given problem instance, we then define two regions of N, according to whether it is larger or smaller than N_c. The two regimes and their implications summarized in Fig. 1(a). In Fig. 1(c) we show the proportion of problems satisfying $\Delta < \delta$ (i.e. $N \leq N_c$) for randomly generated J_{ij} and K_i. We see that the proportion decreases as $\propto 1/N$, which is consistent with the linear scaling of Δ. We note that in the case of atomic ensembles N can be quite large (e.g. 10^3 to 10^{11}) [43, 47], which suggests that for realistic ensemble sizes most of problem instances will be in the regime $N \geq N_c$.

III. SPECTRUM OF THE AQC HAMILTONIAN

So far we have only examined the classical limit of $\lambda = 1$. The overall speed of the AQC will be dependent upon the minimum gap energy with the off-diagonal term (5) present. To illustrate the effect of intermediate λ, we compare the eigenvalue spectrum of the Hamiltonian (3) for the standard qubit case and for $N = 5$ for the same J_{ij} and K_i parameters in Fig. 2(a)(b). The most noticeable difference is the larger number of states when ensembles are used (Fig. 2(b) inset). Despite the larger number of states, plotted on the same energy scale, a non-diminishing gap between ground and excited state maintained for the ensemble case (Fig. 2(b) main figure). This occurs due to the larger energy scale of the ensemble Hamiltonian by a factor of N, which at least partially compensates for the larger number of states. Many of these additional states are logically equivalent states in the sense of (6). For example, we label the states at $\lambda = 1$ in terms of the eigenstates S_i^z. In the qubit version the two lowest states have a spin configuration of $(\sigma_1^z, \sigma_2^z, \sigma_3^z) = (-1, -1, -1)$ and $(+1, -1, -1)$ respectively. In the ensemble version with $N = 5$, the lowest 7 states are all logically equivalent to $(-1, -1, -1)$ in terms of (6). Such logically equivalent states provide protection against diabatic excitations since they occur with energies in the vicinity of the ground state, and act as as a "buffer" before logical errors are induced [38, 40].

Our aim in the AQC will be to keep the adiabatic evolution in the genuine ground state of the ensemble system. Obtaining the ground state and first excited state for the ensemble system in general is a numerically intensive task involving a diagonalization within a Hilbert space of dimension $(N + 1)^M$. To see the behavior for large ensemble sizes, it is desirable to have an approximate method of estimating the gap energy that does not require full diagonalization. Mean field theory provides an accurate estimate of physical quantities for large spin systems. The ensemble nature of the Hamiltonian allows us to extract energies with increasing accuracy particularly for large N. We use a mean field ansatz wavefunction of the form

$$|\Psi_{\rm MF}^{(0)}\rangle = \prod_{i=1}^{M} |0, \theta_i\rangle_i \tag{9}$$

where we define a Fock state of N spins all aligned in the same direction as

$$|0, \theta\rangle_i = \prod_{n=1}^{N} \left(\cos\frac{\theta}{2}|0\rangle_{ni} + \sin\frac{\theta}{2}|1\rangle_{ni} \right). \tag{10}$$

We apply the mean-field ansatz by performing a self-consistent procedure to obtain the parameters θ_i. This is equivalent to taking expectation values of the Hamiltonian (3) with respect to (9) and optimizing for θ_i. From the discussion relating to the logically equivalent states, a suitable mean-field ansatz for the first excited state consists of a spin-wave state where one qubit per ensemble is flipped

$$|\Psi_{\rm MF}^{(1)}\rangle = \sum_{k=1}^{M} \psi_k |1, \theta_k\rangle_k \prod_{i \neq k} |0, \theta_i\rangle_i, \tag{11}$$

where we have defined

$$|1, \theta\rangle = \tilde{S}^x |0, \theta\rangle_i. \tag{12}$$

and $\tilde{S}^x = -\cos\theta S^x + \sin\theta S^z$ creates a single spin flip on an ensemble. To apply the mean-field ansatz (11) we diagonalize an effective Hamiltonian in the ψ_k coefficients and take the lowest energy state (see Appendix C). We note that the mean field theory is only expected to work in the regime with $N \geq N_c$, since the first excited state is taken to be of the form (11), which has a spin configuration that is one spin flip away from the ground state.

The results are shown in Fig. 2(b), where the mean-field estimates (dashed lines) are compared to the exact results. We see that excellent agreement in the energies of the states are obtained with respect to all values of the adiabatic parameter λ. In Fig. 2(c) we plot the exact gap energy for various N in comparison to the mean-field calculation. Figure 2(d) shows the convergence of the energies towards the mean-field results with N at various intermediate values of λ. The mean-field results correspond to the limit $N \to \infty$, and the exactly calculated gaps for various N rapidly approach the mean-field result.

The results of Fig. 2(a)-(d) were for a particular problem instance. What is more meaningful is to study the performance of the scheme for a variety of different problem instances so that the overall behavior can be assessed. We find that the behavior is rather different depending upon whether $N < N_c$ or $N \geq N_c$, due to the different nature of the first excited state. We study the two regimes separately by choosing problem instances where N_c occurs relatively early ($N_c = 2, 3$, Fig. 2(e)) or late ($N_c > 7$, Fig. 2(f)). In Fig. 2(e) we show the average, best, and worst scaling of the minimum gap for problems with $N_c = 2, 3$, such that most of the N-dependence is in the $N \geq N_c$ regime. The best and worst scalings are defined as the largest and smallest difference in the gap comparing the qubit and $N = 7$, the largest ensemble size calculated. We find that the minimum gap increases with N on average. Combined with the logically equivalent buffer states in the region of the ground state, we expect that the AQC performance should improve for these cases.

For the cases with $N_c > 7$ (the $N < N_c$ regime), we see more mixed results (Fig. 2(f)). The average scaling tends to still improve with N, but there are some cases where the minimum gap becomes significantly worse with N. In such cases we expect that the AQC performs poorly. We note that the small values of N considered here are due to limitations in our numerical simulations. We thus expect that for realistic ensemble sizes would satisfy $N \geq N_c$, where the scaling is more favorable.

This may, on first glance, seem to be a counter-intuitive result, since one might expect that with larger N the system should behave more classically. However, it can be seen that in both (4) and (5) the magnitude of the elementary excitation does not diminish as N grows, since it is always a discrete Hamiltonian. Thus the gap does not diminish even for $N \to \infty$, and AQC can be performed with macroscopically sized ensembles.

IV. PERFORMANCE WITH ADIABATIC EVOLUTION

We now directly time-evolve the AQC Hamiltonian and demonstrate its performance. We perform a linear adiabatic sweep such that $\lambda = t/\tau$ and study a fixed set of 60 randomly generated instances for various ensemble sizes N and sweep times τ. We again consider problem Hamiltonians grouped according to $N_c = 2, 3$ or $N_c > 7$, so that we see the $N \geq N_c$ or $N < N_c$ regime respectively. Fig. 3(a)-(d) shows the error probability of finding the state of the system at the end of adiabatic evolution, averaged over random problem instances of J_{ij} and K_i. The error probability is defined as $1 -$ (success probability), where the success probability is defined to be the total probability of all final states that satisfy (6). This includes all logically equivalent states which have the same spin configuration as defined by the sign of the spin operators. This is equivalent to a majority vote decoding of the ensemble states and is similar to error-suppression strategies that have been considered in other works [38, 40].

For problems with $N_c = 2, 3$ (the $N \geq N_c$ regime), for sufficiently long τ, the error probability decreases with N (Fig. 3(a)), as expected from the average increase of the minimum gap as seen in Fig. 2(e). For long adiabatic sweep times τ, we see a very strong decrease of the error — more than would be expected from the increase in the gap as observed in Fig. 2(e). We attribute this to the presence of logically equivalent buffer states as seen in Fig. 2(b). For large N, excitation into the low-lying excited states becomes less harmful because in the regime $N \geq N_c$ they are logically equivalent, as seen in Fig. 1(a). Although we only simulated relatively small system sizes, due to numerical limitations, we expect that for larger N the trend will continue towards lower errors as the gap energy approaches the mean-field value corresponding to $N \to \infty$. On the other hand, for short sweep times τ, the scaling does not improve with N. We attribute this behavior due to the sweep times being in a highly diabatic regime, such that the system is not maintained in the vicinity ground state, which involves high energy excitations. In these cases, since many of the excited states are involved, the increase of the gap does not improve the performance. We note that there did exist rare examples where the error probability scaled badly with N, due to the particular structure of the energy spectrum. However, the occurrence of these poorly scaling examples were so rare that they did not impact the average to a significant extent.

For problems with $N_c > 7$ (the $N < N_c$ regime), the error tends to increase with N (Fig. 3(b)), despite the fact that the average minimum gap increases with N, as seen in Fig. 2(f). We have examined the individual cases and confirmed that for particular cases where the gap increases with N, the error decreases with N as expected. The reason that the average error increases is that the cases with poor gap scaling in Fig. 2(f) tend to have nearly zero success probability, which reduces the average, considerably. Thus the results for problems in the $N < N_c$ regime are mixed and depend very much upon the particular problem instance of whether the gap increases or decreases. We do, however, note that these problem instances themselves rarely occur, as seen in Fig. 1(c), and thus when averaged over all random problem instances, we expect the error to decrease with N.

To see the performance of the AQC in the presence of decoherence, we numerically evolved a master equation in the presence of dephasing for the same problem instances as Fig. 3(a)(b) (see appendix D for details). As seen in Fig. 3(c)(d), we find generally the same behavior of the error with N when decoherence is introduced, but with a higher error probability overall, as expected. For the $N_c = 2, 3$ case in Fig. 3(c), we see that there is generally an improvement of the error with N, particularly for longer sweep times such that adiabaticity is maintained. The new feature here is that there is an optimum sweep time beyond which the error probability starts increasing again. This can be simply explained by noting that the AQC must be performed within the decoherence time available to the computation. Beyond the optimal time, the performance starts to degrade, thus there is a trade-off between maintaining adiabadicity and working within the decoherence time. For the $N_c > 7$ cases in Fig. 3(d), we again see the error increase with N, which is attributed again to particular instances where the minimum gap decreases with N.

The difference in the $N < N_c$ and $N \geq N_c$ regimes is further illustrated for a larger N for a prototypical problem Hamiltonian with $J_{ij} = -1(1 - \delta_{ij})$ and $K_i = K$. This instance has an energy landscape with one global minimum and one local minimum with the spin configuration $S_i^z = -N$ and $S_i^z = N$, for all i. Results including decoherence are shown in Fig. 3(e), together with the N_c values. We see that, as expected, the error probabilities increase in the region $N < N_c$, but sharply decrease exactly at $N = N_c$, and decrease further as N is increased. This can again be attributed to the introduction of logically equivalent buffer states, which act to suppress errors in the AQC.

In addition to randomly generated problem instances, we also examine the Exact Cover 3 problem [2], as an illustration of the compatibility of the Hamiltonian (1) with combinatorial problems. We choose hard Exact Cover 3 instances, which are defined as problems with a unique assignment of values as solutions, corresponding to a non-degenerate ground state of the problem Hamil-

tonian. The scaling of the error with N for various adiabatic sweep times τ is shown in Fig. 3(f) for a typical problem instance. In a similar way to Fig. 3(c), we see again that the error scales favorably with N as long as the sweep time is large enough to maintain adiabaticity but is within the decoherence window. We have verified that similar results are obtained for other generated instances of Exact Cover.

We finally comment on the presence of entanglement during the AQC sweep. The mean field wavefunction as given in (9) takes the form of a product state of spin coherent states on each ensemble. This may suggest that there is no entanglement between the ensembles during the adiabatic evolution. In fact, entanglement is typically present during the evolution, due to the $S_i^z S_j^z$ interaction in the AQC Hamiltonian. The mean-field ground state is merely an approximation to the true ground state, which in fact typically contains entanglement. We have explicitly calculated entanglement for small ensemble sizes (see Appendix E). The presence of entanglement is consistent with past works studying the robustness of entanglement in the presence of decoherence [43–47, 50–52]. The factor of $1/N$ multiplying the $S_i^z S_j^z$ terms makes the type of entangled state of a robust type as discussed in Ref. [50]. We thus expect that the entanglement should survive for macroscopic ensembles within the decoherence window. This can be contrasted to other ensemble-based approaches such as in liquid-state NMR [53, 54], where the entanglement collapses to zero.

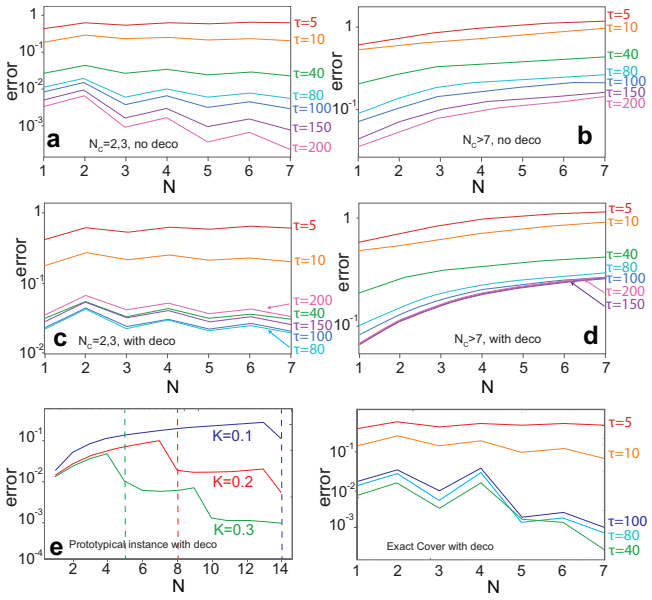

FIG. 3. Error probabilities in the time-evolved adiabatic quantum computation. Averaged error versus N for various τ and $M = 3$ for (a) 60 problem instances with $N_c = 2, 3$; (b) 60 problem instances with $N_c > 7$. Averaged error versus N for various τ and $M = 3$ including dephasing of rate $\Gamma = 10^{-4}$ for the same problem instances with (c) $N_c = 2, 3$; (d) $N_c > 7$. (e) Error for problem instance with $M = 3$, $J_{ij} = -1(1 - \delta_{ij})$ and $K_i = K$, $\Gamma = 10^{-4}$, and $\tau = 100$. Dashed lines indicate the value of N_c for each curve. (f) Error versus N for various τ for a hard Exact Cover instance with $M = 3$ and $\Gamma = 10^{-4}$. The parameters of the Exact Cover instance are $J_{12} = 0.5, J_{13} = 0, J_{23} = 0.5, K_1 = -1, K_2 = -1, K_3 = -1$.

V. CONCLUSIONS AND DISCUSSIONS

In this study, we investigated an equivalent formulation of AQC where qubit ensembles are used instead of qubits, and the ensemble Hamiltonians (4) and (5) are adiabatically evolved. We have found that finding the ground state of (4) is an equivalent problem to the original qubit problem Hamiltonian (1). The main difference of the ensemble and qubit problem Hamiltonians is that the ensemble version introduces many logically equivalent states as defined in (6) with similar energies to the ground state. The introduction of these states is beneficial for AQC since occupation of these states do not cause a logical error, and provide a buffer against diabatic excitation. We found that there are two important regimes with respect to N, depending on the character of the first excited state, summarized in Fig. 1(a). In the regime with $N \geq N_c$, we find that the minimum gap energy increases, and the ground state is logically protected, leading to a reduced error probability in the AQC. In the regime with $N < N_c$, we obtain mixed results, where despite the minimum gap increasing, the AQC scales on average poorly. This was due to the particularly poor performance of the cases where the gap decreases, and can be attributed to the lack of logical protection of the ground state. Once the critical N_c is exceeded, the errors start to decrease again. For realistically large ensemble sizes, all but a minority of problems should satisfy $N \geq N_c$, where the ground state is logically protected.

We thus find that AQC with ensembles should perform well in a great majority of cases for large N. One may find it surprising that it is possible to perform AQC at all with ensembles of qubits, even in the limit of $N \to \infty$. The first key point that allows for the ensemble version to still work is that the discrete nature of the Hamiltonian is preserved under (4) and (5). Thus although the energy of the full space can be viewed as being quasi-continuous as shown in Fig. 1(a), this is only because the space is being viewed in rescaled variables $x_i = S_i^z/N$. Physically, the magnitude of the spins are also growing with N, which preserves the energy gap. From a resource point of view, one may argue that many more physical qubits are being used. However, we take the point of view that the relevant resource is the complexity of the experiment control when dealing with an ensemble as compared to a single qubit. For many implementations the effort required with controlling an ensemble is no more than that of a single qubit. For instance, if performing a single qubit operation on an atom is performed by a laser pulse, then the equivalent ensemble operation is to apply the pulse on the whole ensemble. This is typically

not an operation that costs N times more, since one can illuminate the whole ensemble with the same laser, i.e. it is parallelizable. Thus as long as the operations for the qubit operators $\sigma_i^{x,y,z}$ can be performed with a similar experimental overhead to ensemble operators $S_i^{x,y,z}$, then implementing the ensemble and qubit version of the AQC Hamiltonians should be of comparable complexity.

One may also be concerned that the use of ensembles may be problematic since they could be extremely sensitive to decoherence, owing to their macroscopic nature. The sensitivity of qubit ensemble states have already been investigated in numerous works, see for example Refs. [50, 55–57]. The main point here is that the fragility of the quantum states is state dependent: while Schrodinger cat states are extremely sensitive, spin coherent states are generally quite robust. This is what has allowed the experimental realization of macroscopic quantum states, such as those performed by Polzik and co-workers [43, 44, 52]. The form of the mean-field ground and excited states suggest that the ensemble version of AQC can also be robust for the same reasons. The ground state (9) is nothing but a set of spin coherent states, and (11) is a spin-wave excitation on the ground state. Spin-wave states are also relatively robust and have been demonstrated experimentally before [58]. Therefore, as long as the ensemble size is such that $N \geq N_c$, we believe that it is reasonable to expect that the scheme works even in the presence of decoherence. If it is the case that $N < N_c$, it is less clear what the decoherence properties are since the nature of the state is not yet understood. We nevertheless observe that in some cases the minimum gap can increase, making the ensemble framework viable. While we have not been able to exactly characterize the cases that are most susceptible, we also have not seen any correlation with classically hard instances of combinatorial problems. Considering that these are an extremely small fraction of the full problem set, we find that in most cases the ensemble framework successfully performs error-suppression via the duplication of the quantum information. This is consistent with other approaches using repetition codes with AQC [40, 42].

We have not directly addressed the experimental challenges facing implementation of (4) and (5). The ensemble Hamiltonian could potentially be implemented by numerous physical systems. For the neutral-atom-ensemble implementation [43, 44, 48, 52], all the signs are positive by nature of its construction, as has been analyzed in numerous works before [48, 49, 51, 55]. The Hamiltonians (4) and (5) only involve total spin operators so do not require microscopic control of qubits. The factor of $1/N$ in front of the two-ensemble interaction (4) is also beneficial as it implies only weakly entangling pulses are required to implement it [50]. In the $N \geq N_c$ regime, from the form of the ground state (9), this suggests that highly decoherence-sensitive states are not involved, and this encoding should be robust in the presence of decoherence. These results suggest such ensemble approaches could lead to a practically implementable, error-suppressed version of qubit quantum algorithms.

ACKNOWLEDGMENTS

This work is supported by the Shanghai Research Challenge Fund; New York University Global Seed Grants for Collaborative Research; National Natural Science Foundation of China (61571301); the Thousand Talents Program for Distinguished Young Scholars (D1210036A); and the NSFC Research Fund for International Young Scientists (11650110425); NYU-ECNU Institute of Physics at NYU Shanghai; the Science and Technology Commission of Shanghai Municipality (17ZR1443600); the China Science and Technology Exchange Center(NGA-16-001); and the NSFC-RFBR Collaborative grant (81811530112). J. P. D. would like to acknowledge support from the US Air Force Office of Scientific Research, the Army Research Office, the Defense Advanced Funding Agency, the National Science Foundation, and the Northrop-Grumman Corporation. A. P. acknowledges the RFBR-NSFC collaborative program (Grant No. 18-57-53007).

Appendix A: Implementation with neutral atom ensembles

The basic scheme for implementing the ensemble AQC Hamiltonian can be found in Refs. [48, 49]. Here, an atom chip with multiple trapping sites allows for the creation of ensembles which stores the quantum information on the internal hyperfine ground states of the atom. Neutral atom ensembles have the advantages of excellent coherence properties of the order of minutes [59], and the potential for a massive amount of duplication of the quantum information at the level of $N = 10^3$ or greater [47, 48, 59].

Using standard laser manipulation methods allows for the creation of single ensemble operations creating the S_i^x and S_i^z Hamiltonians. As long as the ensembles are controlled by a common laser field for the whole ensemble, the time resources required to perform such single ensemble operations should be independent of N. The generation of $S_i^z S_j^z$ type interaction [48, 51, 60] and the use of such ensembles for quantum computing has been discussed in numerous past works [49, 55, 57, 61, 62]. We note that we do not consider any on-site interaction terms of the type $(S_i^z)^2$, since we explicitly assume $J_{ii} = 0$. While such terms are often a by-product of the $S_i^z S_j^z$ interaction [51, 63], we assume that such terms can be eliminated by a concatenation with local anti-squeezing [64]. The resources required for implementing an $S_i^z S_j^z$ should again be independent of N. For example, for optical based entanglement methods, as long as the common optical mode couples with both ensembles, the interaction can be produced in a parallel fashion across all the

qubits within the ensembles.

Appendix B: Equivalence of ground states between qubit and ensemble H_Z

1. Equivalence of states at corners of hypercube

Dividing (4) in the main text by N, we obtain

$$E(x_1,\ldots,x_M) = \frac{H_Z}{N} = \sum_{i,j=1}^{M} J_{ij}x_ix_j + \sum_{i=1}^{M} K_ix_i \tag{B1}$$

where we have defined

$$x_i = \frac{S_i^z}{N}. \tag{B2}$$

We will work with rescaled energies E that divide the Hamiltonian (4) in the main text by N. The eigenvalues of S^z take the values $\{-N,-N+2,\ldots,N\}$. Consequently the eigenvalues of x_i take the values $\{-1,-1+2/N,\ldots,1\}$. Comparing (B1) to (1) in the main text, since the eigenvalues of σ_i^z are $\{-1,1\}$, for x_i values taking $\{-1,1\}$ (i.e. the hypercube corners), the same energy is obtained up to a constant factor of N. The spin configurations are thus equivalent in the sense of (7).

2. Variation of the energy along the edge of the hypercube

Let us now see the variation of the energy E where we start from the state that is equivalent to the qubit ground state configuration $x_i = \sigma_i$. The qubit ground state energy is

$$E_0 = \sum_{i,j=1}^{M} J_{ij}\sigma_i\sigma_j + \sum_{i=1}^{M} K_i\sigma_i. \tag{B3}$$

Now parametrize the deviation from the ground state hypercube corner using

$$x_i = \sigma_i(1-2\epsilon_i) \tag{B4}$$

where $\epsilon_i \in [0,1]$. The energy for an arbitrary deviation from the ground state hypercube corner is

$$E(\epsilon_1,\ldots,\epsilon_M) = \sum_{i,j=1}^{M} J_{ij}\sigma_i\sigma_j(1-2\epsilon_i)(1-2\epsilon_j) + \sum_{i=1}^{M} K_i\sigma_i(1-2\epsilon_i). \tag{B5}$$

The energy variation changing just one of the spins x_k gives a rate of change in the energy

$$\frac{\partial E}{\partial \epsilon_k} = -2\sigma_k\left(2\sum_i J_{ik}x_i + K_k\right). \tag{B6}$$

This is a constant with respect to ϵ_k, hence we can observe that the energy variation when changing only one of the spins is always linear. A special case of this when moving along one of the hypercube edges where $x_i = \pm 1$. The variation in energy when moving alone a hypercube edge is always linear.

The ground state configuration corresponds to $\epsilon_i = 0$. Starting from the ground state, the energy variation changing one of the spins is thus

$$E(0,\ldots,0,\epsilon_k,0,\ldots,0) = E_0 + \left.\frac{\partial E}{\partial \epsilon_k}\right|_{\epsilon=0}\epsilon_k. \tag{B7}$$

This corresponds to moving along one of the edges of the hypercube, starting from the equivalent ground state configuration.

Varying ϵ_k from 0 to 1 and keeping all the other $\epsilon_i = 0$ corresponds to flipping one of the spins from $x_k \to -x_k$. This is another hypercube corner, which has an equivalent spin configuration according to the result in Sec. B 1. Since hypercube corners have the same energy E as the original qubit problem, this is guaranteed to have a higher energy since the original state $\epsilon_i = 0$ is by definition the ground state. Combining this with the fact that the energy variation along a hypercube edge is linear, we conclude that

$$\left.\frac{\partial E}{\partial \epsilon_k}\right|_{\epsilon=0} = -2\sigma_k\left(2\sum_i J_{ik}\sigma_i + K_k\right) \geq 0. \tag{B8}$$

The gradient in the vicinity of the ground state is then

$$\nabla E\big|_{\epsilon=0} = \left.\left(\frac{\partial E}{\partial \epsilon_1}, \frac{\partial E}{\partial \epsilon_2}, \ldots, \frac{\partial E}{\partial \epsilon_M}\right)\right|_{\epsilon=0}. \tag{B9}$$

The energy variation in an arbitrary direction starting from the ground state corner is therefore given by

$$E(\epsilon_1,\epsilon_2,\ldots,\epsilon_M) \approx E_0 + \nabla E\big|_{\epsilon=0}\cdot(\epsilon_1,\epsilon_2,\ldots,\epsilon_M). \tag{B10}$$

From (B8), since each of the derivatives are positive, we can conclude that the gradient of the energy in an arbitrary direction in the vicinity of the ground state will always be positive.

3. Variation of energy from the ground state to an arbitrary hypercube corner

The previous section shows that the energy increases in an arbitrary direction starting from the ground state

corner. We also showed that varying the energy along an hypercube edge changes the energy linearly. We now examine the energy variation starting from the ground state hypercube corner to an arbitrary hypercube corner. A linear trajectory connecting the ground state corner to an arbitrary corner is defined by

$$\epsilon_i = n_i \varepsilon \tag{B11}$$

where $n_i \in \{0, 1\}$ are integer parameters which determine the trajectory and $\varepsilon \in [0, 1]$ is the parameter which determines the position along the chosen trajectory.

Substituting (B11) and (B4) into (B1) and subtracting off the ground state (B3), we obtain

$$\begin{aligned} f_{n_1 \ldots n_M}(\varepsilon) &= E(x_1, \ldots, x_M) - E_0 \\ &= -4 \sum_{i,j} J_{ij} \sigma_i \sigma_j \left(n_i \varepsilon - n_i n_j \varepsilon^2 \right) - 2 \sum_i K_i \sigma_i n_i \varepsilon. \end{aligned} \tag{B12}$$

We know that when $\varepsilon = 1$, this corresponds to another hypercube corner. From the result of Sec. B 1, this must have a higher energy since $\varepsilon = 0$ has by definition the same energy as the qubit ground state. Furthermore, we observe from (B12) that the variation is always a quadratic polynomial with respect to ε.

We now show that there is no other lower energy state along the line connecting the ground state to another hypercube corner. From the fact that the energy gradient is positive from (B8), and the energy varies quadratically, there are only two possibilities for the type of curve that (B12) follows with respect to ε. First consider the case that the parabola in ε is concave upwards, namely

$$\sum_{i,j} J_{ij} \sigma_i \sigma_j n_i n_j \geq 0. \tag{B13}$$

Since the energy gradient at $\varepsilon = 0$ is positive, the turning point must occur for $\varepsilon < 0$ and we can deduce that the energy monotonically increases to the hypercube corner. In the case that the parabola is concave downwards, namely

$$\sum_{i,j} J_{ij} \sigma_i \sigma_j n_i n_j < 0, \tag{B14}$$

then for the same reasons, this means that the turning point occurs for $\epsilon > 0$. Since the hypercube corner with $\varepsilon = 1$ is at a higher energy than the ground state, the energy rises monotonically if the turning point is $\varepsilon \geq 1$. If the turning point is $0 < \epsilon < 1$, the energy increases, then decreases and there is a maximum in the energy between the hypercube corners. In all the cases the minimum is at the ground state hypercube corner, i.e. $\varepsilon = 0$.

Since $f_{n_1 \ldots n_M}(\varepsilon = 0) = 0$ by construction, the above result implies that

$$f_{n_1 \ldots n_M}(\varepsilon) \geq 0. \tag{B15}$$

4. Variation of energy from the ground state in an arbitrary direction

We have so far shown that energy of any of the points along the trajectory connecting the ground state hypercube corner to any other hypercube corner is higher or the same as the ground state energy E_0. To show an arbitrary point in the hypercube also has a higher energy than E_0, we should connect the ground state along an arbitrary trajectory through the hypercube. This can be parameterized by

$$\epsilon_i = \alpha_i \varepsilon. \tag{B16}$$

where in this case $\alpha_i \in [0, 1]$ are continuous parameters that determine the trajectory. In order to have $\varepsilon \in [0, 1]$ be the full range of the trajectory, we demand that at least one of the α_i be equal to unity, i.e.

$$\sup_i \alpha_i = 1. \tag{B17}$$

The energy variation along this trajectory can be calculated in a similar way to (B12), and is given by

$$\begin{aligned} F(\varepsilon) &= E(x_1, \ldots, x_M) - E_0 \\ &= -4 \sum_i \sum_{j \neq i} J_{ij} \sigma_i \sigma_j \left(\alpha_i \varepsilon - \alpha_i \alpha_j \varepsilon^2 \right) - 2 \sum_i K_i \sigma_i \alpha_i \varepsilon \\ &= \sum_i \sum_{j \neq i} D_{ij}(\varepsilon) \alpha_i \alpha_j + \sum_i C_i \alpha_i, \end{aligned} \tag{B18}$$

where we have defined

$$\begin{aligned} D_{ij}(\varepsilon) &= 4 \varepsilon^2 J_{ij} \sigma_i \sigma_j, \\ C_i(\varepsilon) &= -2 \varepsilon \left(K_i \sigma_i + 2 \sum_{j \neq i} J_{ij} \sigma_i \sigma_j \right), \end{aligned} \tag{B19}$$

and used the fact that $J_{ii} = 0$.

We would like to show that $F(\varepsilon) \geq 0$ for any choice of α_i, which would show that a state along an arbitrary trajectory starting from the ground state hypercube corner always has a higher or the same energy. To achieve this, we construct the function $F(\varepsilon)$ with a linear combination of the basis functions $f_{n_1 \ldots n_M}(\varepsilon)$. That is, we require coefficients such that

$$F(\varepsilon) = \sum_{n_1, \ldots, n_M} w_{n_1 \ldots n_M} f_{n_1 \ldots n_M}(\varepsilon), \tag{B20}$$

where $n_i \in \{0, 1\}$. Since the basis functions are individually positive (B12), it then follows that if

$$w_{n_1 \ldots n_M} \geq 0, \tag{B21}$$

then $F(\varepsilon) \geq 0$.

Substituting (B12) and (B18) into (B20), we obtain

$$\sum_{n_1,\ldots,n_M} w_{n_1\ldots n_M} f_{n_1\ldots n_M}(\varepsilon) = \sum_i \sum_{j\neq i} D_{ij}(\varepsilon) \sum_{n_1,\ldots,n_M} w_{n_1\ldots n_M} n_i n_j + \sum_i C_i(\varepsilon) \sum_{n_1,\ldots,n_M} w_{n_1\ldots n_M} n_i. \quad \text{(B22)}$$

Comparing (B22) and (B18) we observe that firstly the coefficients must satisfy for $i \neq j$

$$\sum_{n_1,\ldots,n_M} w_{n_1\ldots n_M} n_i n_j = \alpha_i \alpha_j. \quad \text{(B23)}$$

This is a set of $M^2 - M$ linear equations to be solved with 2^M variables. There are more degrees of freedom than equations, hence will typically be many choices of $w_{n_1\ldots n_M}$ that satisfy (B23). Here we note that in this sum, any n_i which has a single "1" and all others "0"

$$\sum_i n_i = 1, \quad \text{(B24)}$$

does not contribute due to the product $n_i n_j$, noting that $i \neq j$.

We also require that

$$\sum_{n_1,\ldots,n_M} w_{n_1\ldots n_M} n_i = \alpha_i, \quad \text{(B25)}$$

which is another set of M equations to be satisfied. This set of equations can be reduced to an inequality using the fact that the n_i of the form (B24) do not contribute to the sum (B23). Thus as long as we have

$$\sum_{\substack{n_1,\ldots,n_M \\ (\sum_i n_i > 1)}} w_{n_1\ldots n_M} n_i \leq \alpha_i, \quad \text{(B26)}$$

then we can always choose positive

$$w_{0\ldots010\ldots0} = \alpha_i - \sum_{\substack{n_1,\ldots,n_M \\ \sum_i n_i > 1}} w_{n_1\ldots n_M} n_i, \quad \text{(B27)}$$

to satisfy (B25), where $w_{0\ldots010\ldots0}$ is the coefficient with $n_i = 1$ and all other $n_j = 0$, $j \neq i$.

In summary, we must look for coefficients $w_{n_1\ldots n_M}$ such that (B23) is satisfied under the constraints of (B26) and (B21). The existence of such a solution can be shown using Farkas' lemma. Let us begin by formulating our problem in terms of a linear program of the form

$$\sum_{0<k<2^M} w_k n_i(k) n_j(k) = \alpha_i \alpha_j \quad (i,j) \in [0,M]^2, \quad \text{(B28)}$$

$$\sum_{0<k<2^M} w_k n_i(k) \leq \alpha_i \quad 0 \leq i \leq M, \quad \text{(B29)}$$

$$w_k \geq 0 \quad 0 \leq k < 2^M. \quad \text{(B30)}$$

Here we have relabeled the indices $n_1 \ldots n_M \to k$ where

$$k = \sum_{j=1}^{M} 2^{j-1} n_j \quad \text{(B31)}$$

is the integer corresponding to the binary number $n_1 \ldots n_M$. The function $n_j(k)$ returns the jth digit of binary representation of integer number k.

This problem can be re-written in canonical form, in matrix notation $Aw \leq b$, where A is a matrix of coefficients and b is a vector corresponding to right hand side of the constraints:

$$\sum_{0<k<2^M} w_k n_i(k) n_j(k) \leq \alpha_i \alpha_j \quad (i,j) \in [0,M]^2, \quad \text{(B32)}$$

$$-\sum_{0<k<2^M} w_k n_i(k) n_j(k) \leq -\alpha_i \alpha_j \quad (i,j) \in [0,M]^2, \quad \text{(B33)}$$

$$\sum_{0<k<2^M} w_k n_i(k) \leq \alpha_i \quad 0 \leq i \leq M, \quad \text{(B34)}$$

$$-w_k \leq 0 \quad 0 \leq k < 2^M \quad \text{(B35)}$$

This representation is semantically equivalent to the representation (B28), (B29), (B30) but has an advantage of having each constraint in the same form. From now on we will refer to this definition as the primal problem.

To prove that primal problem always has a solution we will use Farkas' lemma in the form as stated in Ref. [65], that a solution to $Aw \leq b$ exists if and only if an associated dual problem in the form

$$u^T A = 0, \quad u \geq 0, \quad u^T b < 0, \quad \text{(B36)}$$

has no solution. To apply this technique we need to construct the dual problem starting from the primal problem and then show that the dual problem has no solution, or in other words, is infeasible.

Variables in the primal problem are represented by vector w, and in the dual problem are represented by the vector u. It is important to note the domains of those variables are not the same as in the dual problem we require $u \geq 0$. From the definition of Farkas' lemma we can deduce that dual problem has as many variables as primal problem had rows and as many equality constraints as primal problem has variables. This indicates that the dual problem must have $2M^2 + M + 2^M$ columns, $u^T A = 0$ creates 2^M rows which are equality constraints and $u^T b < 0$ creates a single row that corresponds to a constraint of the form < 0 that has only α_i values as coefficients. From this definition we can also see that each row of primal gives a column in the dual, if we group terms we deduce that (B32) and (B33) will give us difference of terms with same coefficients, (B34) will give us a term that is present in $2^M - M$ rows as it vanishes for M

rows, and finally, (B35) will add a distinct variable at the end of each row. We can represent those relevant column groups using the variables $u_{ij}^{(1)}$, $u_{ij}^{(2)}$, $u_i^{(3)}$ and $u_k^{(4)}$ corresponding to following rows in the primal problem (B32), (B33), (B34) and (B35) respectively. We also recall that $0 < k < 2^M$.

This gives us enough information to state the dual problem as follows:

$$\sum_{\substack{i,j\\i\neq j}}^{M} n_i(k)n_j(k)u_{ij}^{(1)} - \sum_{\substack{i,j\\i\neq j}}^{M} n_i(k)n_j(k)u_{ij}^{(2)} + \sum_{i}^{M} n_i(k)u_i^{(3)} - u_k^{(4)} = 0, \tag{B37}$$

$$\sum_{\substack{i,j\\i\neq j}}^{M} \alpha_i\alpha_j u_{ij}^{(1)} - \sum_{\substack{i,j\\i\neq j}}^{M} \alpha_i\alpha_j u_{ij}^{(2)} + \sum_{i}^{M} \alpha_i u_i^{(3)} < 0. \tag{B38}$$

In the primal problem, as mentioned earlier, value of $n_i(k)$ depends on the value k which is associated to column variable w_k. In the dual problem, the value of k is associated to the row number of the problem. Since $n_i(k)$ still depends on k, each row in the dual problem has $n_i(k)$ corresponding to the same binary string. We can rewrite it to more compact form by adding $u_k^{(4)}$ to both sides of (B37). Since $u \geq 0$ it relaxes those constraints from equality constraints into constraints that must be greater or equal to zero. To improve readability, let us also factor out the sum coefficients to give

$$\sum_{\substack{i,j\\i\neq j}}^{M} n_i(k)n_j(k)(u_{ij}^{(1)} - u_{ij}^{(2)}) + \sum_{i}^{M} n_i(k)u_i^{(3)} \geq 0, \tag{B39}$$

$$\sum_{\substack{i,j\\i\neq j}}^{M} \alpha_i\alpha_j(u_{ij}^{(1)} - u_{ij}^{(2)}) + \sum_{i}^{M} \alpha_i u_i^{(3)} < 0. \tag{B40}$$

This is a complete dual problem, however we do not need all the constraints to be violated to show dual is infeasible. Showing that one of the instances is violated is sufficient to show that the dual problem has no solution. For convenience we choose the case $k = 2^M - 1$, which corresponds to $n_j = 1$ for all j:

$$\sum_{\substack{i,j\\i\neq j}}^{M} (u_{ij}^{(1)} - u_{ij}^{(2)}) + \sum_{i}^{M} u_i^{(3)} \geq 0, \tag{B41}$$

$$\sum_{\substack{i,j\\i\neq j}}^{M} \alpha_i\alpha_j(u_{ij}^{(1)} - u_{ij}^{(2)}) + \sum_{i}^{M} \alpha_i u_i^{(3)} < 0. \tag{B42}$$

Since both constraints (B41) and (B42) have same value on their right hand side, we can relate them to each other, then we subtract (B41) from all terms

$$\sum_{\substack{i,j\\i\neq j}}^{M} (\alpha_i\alpha_j - 1)(u_{ij}^{(1)} - u_{ij}^{(2)}) + \sum_{i}^{M} (\alpha_i - 1)u_i^{(3)} < \sum_{\substack{i,j\\i\neq j}}^{M} (0-1)(u_{ij}^{(1)} - u_{ij}^{(2)}) + \sum_{i}^{M} (0-1)u_i^{(3)} \leq 0. \tag{B43}$$

We can see that (B43) cannot be true because $0 \leq \alpha_i \leq 1$, which shows that constraint (B37) with $k = 2^M - 1$ is in conflict with constraint (B38). This shows that the dual problem is not feasible, and therefore by Farkas' lemma, the primal problem is always feasible.

Appendix C: Mean-field theory of the adibatic quantum computing Hamiltonian

1. Ground state by self-consistent iteration

In this section we derive a mean-field theory of the Hamiltonian (3) of the main text, using the ensemble Hamiltonians (4) and (5). Mean-field theory amounts making the substitution

$$S_i^z = \langle S_i^z \rangle + \delta S_i^z \tag{C1}$$

where $\delta S_i^z = S_i^z - \langle S_i^z \rangle$. The averages $\langle S_i^z \rangle$ are unknown at this stage but will be determined later. Substituting (C1) into (3) of the main text, and discarding second and higher order terms in δS_i^z, we obtain

$$H_{\mathrm{MF}}^{(0)} = \sum_{i=1}^{M} [-(1-\lambda)S_i^x + \lambda(2M_i + K_i)S_i^z] - \frac{\lambda}{N}\sum_{ij} J_{ij}\langle S_i^z\rangle\langle S_j^z\rangle. \tag{C2}$$

where

$$M_i = \frac{1}{N}\sum_j J_{ij}\langle S_j^z\rangle. \tag{C3}$$

The Hamiltonian (C2) can be diagonalized by the transformation

$$H_{\mathrm{MF}}^{(0)} = -\sum_{i=1}^{M} \sqrt{(1-\lambda)^2 + \lambda^2(2M_i + K_i)^2}\,\tilde{S}_i^z - \frac{\lambda}{N}\sum_{ij} J_{ij}\langle S_i^z\rangle\langle S_j^z\rangle \tag{C4}$$

where

$$\tilde{S}_i^z = \sin\phi_i S_i^x + \cos\phi_i S_i^z \tag{C5}$$

and

$$\sin\phi_i = \frac{1-\lambda}{\sqrt{(1-\lambda)^2+\lambda^2(2M_i+K_i)^2}}$$
$$\cos\phi_i = \frac{-\lambda(2M_i+K_i)}{\sqrt{(1-\lambda)^2+\lambda^2(2M_i+K_i)^2}}. \quad \text{(C6)}$$

The ground state solution of this Hamiltonian takes the general form

$$|\Psi^{(0)}_{\rm MF}\rangle = \prod_{i=1}^{M} |0,\theta_i\rangle_i \quad \text{(C7)}$$

where the state $|0,\theta_i\rangle_i$ is defined in (10) of the main text. This gives the mean-field ansatz of (9) in the main text.

The parameters θ_i are found such that the ensembles are maximally polarized, demanding that

$$\tilde{S}^z_i|0,\theta_i\rangle_i = N|0,\theta_i\rangle_i. \quad \text{(C8)}$$

This is satisfied by taking $\theta_i = \phi_i$, or

$$|0,\theta_i\rangle_i = \prod_{n=1}^{N}\left(\cos\frac{\phi_i}{2}|0\rangle_{ni} + \sin\frac{\phi_i}{2}|1\rangle_{ni}\right). \quad \text{(C9)}$$

Since the angles ϕ_i in (C6) involve the unknown expectation values $\langle S^z_i\rangle$, this still does not constitute a solution. The find the $\langle S^z_i\rangle$, we use the solution (C7) and (C9) to evaluate the expectation value

$$\langle S^z_i\rangle = N\cos\phi_i. \quad \text{(C10)}$$

Using the expression (C6) we obtain the self-consistent equation

$$x_i = \frac{-\lambda(2M_i+K_i)}{\sqrt{(1-\lambda)^2+\lambda^2(2M_i+K_i)^2}} \quad \text{(C11)}$$

where we have used the parametrization $x_i = \langle S^z_i\rangle/N$. The parameter $x_i \in [-1,1]$ according to the current definition. Using the result that the ground state for the qubit and ensemble Hamiltonians are equivalent, we may further parameterize

$$z_i = \sigma_i x_i = \frac{\langle S^z_i\rangle\sigma_i}{N} \quad \text{(C12)}$$

such that we expect that $z_i \in [0,1]$. Here σ_i is the ground state configuration for the qubit Hamiltonian H_Z. The self-consistent equation in terms of z_i then reads

$$z_i = \frac{-\sigma_i\lambda(2M_i+K_i)}{\sqrt{(1-\lambda)^2+\lambda^2(2M_i+K_i)^2}} \quad \text{(C13)}$$

where

$$M_i = \sum_j J_{ij}\sigma_j z_j. \quad \text{(C14)}$$

The ground state energy according to (C4) is then

$$E^{(0)}_{\rm MF} = -N\sum_{i=1}^{M}\sqrt{(1-\lambda)^2+\lambda^2(2M_i+K_i)^2} - N\lambda\sum_{ij}J_{ij}\sigma_i\sigma_j z_i z_j. \quad \text{(C15)}$$

2. Ground state by optimization

An equivalent procedure to obtain the ground state is simply to treat (C7) as an ansatz wavefunction and optimize for the parameters θ_i. Evaluating the expectation value with respect to the Hamiltonian (3) of the main text, using the ensemble Hamiltonians (4) and (5) yields

$$\begin{aligned} E^{(0)}_{\rm MF} &= \langle\Psi^{(0)}_{\rm MF}|H|\Psi^{(0)}_{\rm MF}\rangle \\ &= -N(1-\lambda)\sum_{i=1}^{M}\sin\theta_i \\ &\quad + N\lambda\left(\sum_{ij}J_{ij}\cos\theta_i\cos\theta_j + \sum_i K_i\cos\theta_i\right). \end{aligned} \quad \text{(C16)}$$

The equivalent parametrization to (C12) corresponds to

$$\begin{aligned} \cos\theta_i &= z_i\sigma_i \\ \sin\theta_i &= \sqrt{1-z_i^2}, \end{aligned} \quad \text{(C17)}$$

where σ_i are the ground state spin configurations for the qubit Hamiltonian, and we used the fact that

$$\langle\Psi^{(0)}_{\rm MF}|S^z_i|\Psi^{(0)}_{\rm MF}\rangle = N\cos\theta_i. \quad \text{(C18)}$$

The ground state energy can then be written as

$$\begin{aligned} E^{(0)}_{\rm MF} &= -N(1-\lambda)\sum_{i=1}^{M}\sqrt{1-z_i^2} \\ &\quad + N\lambda\left(\sum_{ij}J_{ij}\sigma_i\sigma_j z_i z_j + \sum_i K_i\sigma_i z_i\right). \end{aligned} \quad \text{(C19)}$$

This expression is optimized for $z_i \in [0,1]$

This yields the same results as the self-consistent procedure in the previous section. The self-consistent solution tends to numerically give faster results and hence this is used for our computations.

3. First excited state and gap energy

To obtain the gap, we require also an estimation of the first excited state. To deduce the form of this, first let us consider several limiting cases.

In the limit $\lambda = 1$, for parameters such that (8) in the main text is the gap energy (i.e. $\delta < \Delta$), the first excited state takes the form

$$|1,\frac{(\sigma_k+1)\pi}{2}\rangle_k \prod_{i\neq k}|0,\frac{(\sigma_i+1)\pi}{2}\rangle_i \quad \text{(C20)}$$

where k is the minimal value found in (8) in the main text. Here we defined the spin coherent states with one

of the spins flipped as

$$\begin{aligned}|1,\theta\rangle =&\tilde{S}_i^x|0,\theta\rangle \\ =&\frac{1}{\sqrt{N}}\sum_{k=1}^{N}(\sin\theta|0\rangle_k-\cos\theta|1\rangle_k) \\ &\otimes\prod_{n\neq k}(\cos\theta|0\rangle_n+\sin\theta|1\rangle_n)\,. \end{aligned} \tag{C21}$$

where $\tilde{S}_i^x = -\cos\theta S_i^x + \sin\theta S_i^z$. The flipped spin is a symmetric superposition across the whole ensemble in (C21). We work in the symmetric subspace because the adiabatic quantum computing Hamiltonian (4) and (5) in the main text only involves symmetric operators.

In the reverse limit of $\lambda = 0$, the first excited state is the state with a single spin flip on one of the ensembles

$$|1,\frac{\pi}{2}\rangle_j\prod_{i\neq j}\left(|0,\frac{\pi}{2}\rangle_i\right). \tag{C22}$$

The first excited state for (C22) is M-fold degenerate, the ensemble with the flipped spin can be any one of $j \in [1, M]$.

For small but non-zero $\lambda > 0$, the H_Z will break the degeneracy of the ensemble with the flipped spin. The lowest energy state will be a superposition of the terms of the form (C22). This suggests that we use a mean-field ansatz for the first excited state as

$$|\Psi_{\rm MF}^{(1)}\rangle = \sum_{k=1}^{M}\psi_k|1,\theta_k\rangle_k\prod_{i\neq k}|0,\theta_i\rangle_i, \tag{C23}$$

which gives the expression in the main text.

We now describe how to find the parameters in (C23). For the parameters θ_i, as the state is a perturbation of the ground state (C7), we simply use the same parameters found in the self-consistent calculation of the ground state. The ψ_k can be found by constructing a matrix in the basis

$$|\psi_k\rangle = |1,\theta_k\rangle_k\prod_{i\neq k}|0,\theta_i\rangle_i \tag{C24}$$

which form an orthogonal set of basis states. The diagonal matrix elements of the $M \times M$ matrix can be computed to be

$$\begin{aligned}\langle\psi_k|H|\psi_k\rangle =&E_{\rm MF}^{(0)}+2(1-\lambda)\sin\theta_k-2\lambda K_k\cos\theta_k \\ &-4\lambda\sum_{i\neq k}J_{ik}\cos\theta_i\cos\theta_k \end{aligned} \tag{C25}$$

where $E_{\rm MF}^{(0)}$ is the expression for the ground state energy (C16), and we used the fact that $J_{ij} = J_{ji}$ and $J_{ii} = 0$. In terms of the parametrization (C17), the diagonal terms are

$$\begin{aligned}\langle\psi_k|H|\psi_k\rangle =&E_{\rm MF}^{(0)}+2(1-\lambda)\sqrt{1-z_k^2}-2\lambda K_k\sigma_k z_k \\ &-4\lambda\sum_{i\neq k}J_{ik}\sigma_i\sigma_k z_i z_k \end{aligned} \tag{C26}$$

and the expression for the ground state (C19) is used for $E_{\rm MF}^{(0)}$. The off-diagonal terms are

$$\langle\psi_{k'}|H|\psi_k\rangle =2\lambda J_{kk'}\sin\theta_k\sin\theta_{k'}. \tag{C27}$$

In terms of the parametrization (C17), this can be written

$$\langle\psi_{k'}|H|\psi_k\rangle =2\lambda J_{kk'}\sqrt{1-z_k^2}\sqrt{1-z_{k'}^2}. \tag{C28}$$

To calculate the first excited state energy, we diagonalize the matrix defined by (C26) and (C28) and take the smallest eigenvalue. Equivalently, the gap can be directly found by subtracting the ground state energy $E_{\rm MF}^{(0)}$ from (C26), diagonalizing the matrix, and taking the minimum eigenvalue.

Appendix D: Decoherence

To examine the performance of the ensemble version of AQC under decoherence, we consider the specific case of S^z-dephasing. We choose the S^z basis for the dephasing since it is likely to have the largest effect on the AQC, since the initial state are ensembles polarized in the S^x-basis. It is known that S^z-dephasing will cause a collapse of Schrodinger cat state superpositions with an enhancement of N^2 [50], and if such states appear during the evolution, it will strongly affect the AQC. We use the master equation [66]

$$\frac{d\rho}{dt} = i[\rho, H] - \frac{\Gamma}{2}\sum_{n=1}^{M}[\rho(S_n^z)^2 - 2S_n^z\rho S_n^z + (S_n^z)^2\rho] \tag{D1}$$

where Γ is the dephasing rate and H is the Hamiltonian (3) with (4) and (5) in the main text. Starting from the eigenstate of the initial Hamiltonian we solved the master equation numerically for the combined adiabatic and dephasing evolution. The performance of the AQC is then evaluated through the probability of finding the state of the system in the ground state at the end of the adiabatic evolution. Qutip was used for the simulations [67].

Appendix E: Ensemble-ensemble entanglement

The mean-field ground state Eq. (9) in the main text is explicitly of the form of a product state, which suggests that there is zero entanglement between the ensembles at all times in the adiabatic evolution. This is in fact an artifact of the mean-field approximation, and typically there will be entanglement between the ensembles. In Fig. 4 we show the entanglement between two ensembles as characterized by the logarithmic negativity [68, 69] during the adiabatic sweep. We see that as the ensemble size is increased, the entanglement does not diminish and approaches a common curve. This is consistent with prior

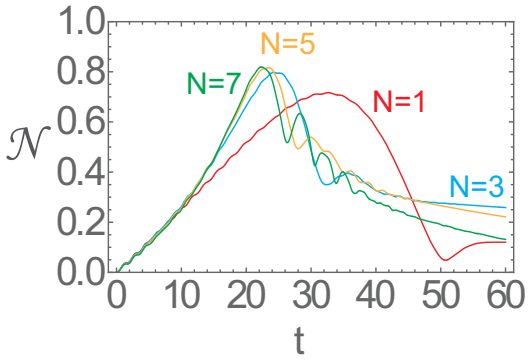

FIG. 4. Entanglement between ensembles in an adiabatic evolution. The logarithmic negativity $\mathcal{N} = \log_2 ||\rho^{T_2}||$ is calculated for the $M = 2$ case for $J_{ij} = -1(1 - \delta_{ij})$, $K_i = 0.1$, an adiabatic sweep time of $\tau = 60$, and dephasing rate of $\Gamma = 10^{-4}$.

studies relating to the robustness of entanglement in such ensembles in the presence of decoherence. The basic result is that for interaction times of the $S_i^z S_j^z$ Hamiltonian of the order $t \sim 1/N$, the entanglement survives robustly in the limit of $N \to \infty$ [50]. Due to the factor of $1/N$ in the ensemble Hamiltonian H_Z, the class of entanglement that is created by the AQC Hamiltonian is expected to be similar.

[1] E. Farhi, J. Goldstone, S. Gutmann, and M. Sipser, arXiv preprint quant-ph/0001106 (2000).
[2] E. Farhi, J. Goldstone, S. Gutmann, J. Lapan, A. Lundgren, and D. Preda, Science **292**, 472 (2001).
[3] A. Das and B. K. Chakrabarti, Rev. Mod. Phys. **80**, 1061 (2008).
[4] T. Albash and D. A. Lidar, Rev. Mod. Phys. **90**, 015002 (2018).
[5] A. Finnila, M. Gomez, C. Sebenik, C. Stenson, and J. Doll, Chemical physics letters **219**, 343 (1994).
[6] T. Kadowaki and H. Nishimori, Physical Review E **58**, 5355 (1998).
[7] G. E. Santoro, R. Martoňák, E. Tosatti, and R. Car, Science **295**, 2427 (2002).
[8] J. Brooke, D. Bitko, G. Aeppli, et al., Science **284**, 779 (1999).
[9] M. Mézard, G. Parisi, and M. Virasoro, *Spin glass theory and beyond: An Introduction to the Replica Method and Its Applications*, vol. 9 (World Scientific Publishing Company, 1987).
[10] C. H. Papadimitriou, *Computational Complexity* (Pearson, 1995).
[11] D. S. Garey, Michael R.; Johnson, *Computers and Intractability: A Guide to the Theory of NP-Completeness* (W.H. Freeman, 1979).
[12] W. Van Dam, M. Mosca, and U. Vazirani, in *Foundations of Computer Science, 2001. Proceedings. 42nd IEEE Symposium on* (IEEE, 2001), pp. 279–287.
[13] J. Roland and N. J. Cerf, Physical Review A **65**, 042308 (2002).
[14] T. Hogg, Physical Review A **67**, 022314 (2003).
[15] M. Amin, Physical review letters **100**, 130503 (2008).
[16] A. M. Childs, E. Farhi, and J. Preskill, Physical Review A **65**, 012322 (2001).
[17] M. Sarandy and D. Lidar, Physical review letters **95**, 250503 (2005).
[18] J. Roland and N. J. Cerf, Physical Review A **71**, 032330 (2005).
[19] D. A. Lidar, Physical Review Letters **100**, 160506 (2008).
[20] S. Ashhab, J. Johansson, and F. Nori, Physical Review A **74**, 052330 (2006).
[21] M. H. Amin, D. V. Averin, and J. A. Nesteroff, Physical Review A **79**, 022107 (2009).
[22] Q. Deng, D. V. Averin, M. H. Amin, and P. Smith, Scientific reports **3**, 1479 (2013).
[23] D. Aharonov and A. Ta-Shma, in *Proceedings of the thirty-fifth annual ACM symposium on Theory of computing* (ACM, 2003), pp. 20–29.
[24] A. Mizel, D. A. Lidar, and M. Mitchell, Physical review letters **99**, 070502 (2007).
[25] D. Aharonov, W. Van Dam, J. Kempe, Z. Landau, S. Lloyd, and O. Regev, SIAM review **50**, 755 (2008).
[26] Z. Wei and M. Ying, Physics Letters A **354**, 271 (2006).
[27] M. Steffen, W. van Dam, T. Hogg, G. Breyta, and I. Chuang, Physical Review Letters **90**, 067903 (2003).
[28] A. Mitra, A. Ghosh, R. Das, A. Patel, and A. Kumar, Journal of Magnetic Resonance **177**, 285 (2005).
[29] M. W. Johnson, M. H. Amin, S. Gildert, T. Lanting, F. Hamze, N. Dickson, R. Harris, A. J. Berkley, J. Johansson, P. Bunyk, et al., Nature **473**, 194 (2011).
[30] S. Boixo, T. Albash, F. M. Spedalieri, N. Chancellor, and D. A. Lidar, Nature communications **4**, 2067 (2013).
[31] R. Barends, A. Shabani, L. Lamata, J. Kelly, A. Mezzacapo, U. Las Heras, R. Babbush, A. G. Fowler, B. Campbell, Y. Chen, et al., Nature **534**, 222 (2016).
[32] S. W. Shin, G. Smith, J. A. Smolin, and U. Vazirani, arXiv preprint arXiv:1401.7087 (2014).
[33] S. Boixo, T. F. Rønnow, S. V. Isakov, Z. Wang, D. Wecker, D. A. Lidar, J. M. Martinis, and M. Troyer, Nature Physics **10**, 218 (2014).
[34] T. F. Rønnow, Z. Wang, J. Job, S. Boixo, S. V. Isakov, D. Wecker, J. M. Martinis, D. A. Lidar, and M. Troyer, Science **345**, 420 (2014).
[35] T. Albash, T. F. Rønnow, M. Troyer, and D. A. Lidar, The European Physical Journal Special Topics **224**, 111 (2015).
[36] B. Heim, T. F. Rønnow, S. V. Isakov, and M. Troyer, Science **348**, 215 (2015).
[37] J. Preskill, preprint arXiv:1801.00862 (2018).

[38] K. C. Young, M. Sarovar, and R. Blume-Kohout, Physical Review X **3**, 041013 (2013).

[39] M. Sarovar and K. C. Young, New Journal of Physics **15**, 125032 (2013).

[40] K. L. Pudenz, T. Albash, and D. A. Lidar, Nature communications **5**, 3243 (2014).

[41] S. P. Jordan, E. Farhi, and P. W. Shor, Physical Review A **74**, 052322 (2006).

[42] W. Vinci, T. Albash, and D. A. Lidar, npj Quantum Information **2**, 16017 (2016).

[43] B. Julsgaard, A. Kozhekin, and E. S. Polzik, Nature **413**, 400 (2001).

[44] J. F. Sherson, H. Krauter, R. K. Olsson, B. Julsgaard, K. Hammerer, I. Cirac, and E. S. Polzik, Nature **443**, 557 (2006).

[45] P. Kunkel, M. Prüfer, H. Strobel, D. Linnemann, A. Frölian, T. Gasenzer, M. Gärttner, and M. K. Oberthaler, Science **360**, 413 (2018).

[46] K. Lange, J. Peise, B. Lücke, I. Kruse, G. Vitagliano, I. Apellaniz, M. Kleinmann, G. Tóth, and C. Klempt, Science **360**, 416 (2018).

[47] M. Fadel, T. Zibold, B. Décamps, and P. Treutlein, Science **360**, 409 (2018).

[48] A. Abdelrahman, T. Mukai, H. Häffner, and T. Byrnes, Optics express **22**, 3501 (2014).

[49] T. Byrnes, D. Rosseau, M. Khosla, A. Pyrkov, A. Thomasen, T. Mukai, S. Koyama, A. Abdelrahman, and E. Ilo-Okeke, Optics Communications **337**, 102 (2014).

[50] T. Byrnes, Phys. Rev. A **88**, 023609 (2013).

[51] A. N. Pyrkov and T. Byrnes, New Journal of Physics **15**, 093019 (2013).

[52] K. Hammerer, A. S. Sørensen, and E. S. Polzik, Rev. Mod. Phys. **82**, 1041 (2010).

[53] N. C. Menicucci and C. M. Caves, Phys. Rev. Lett. **88**, 167901 (2002).

[54] S. L. Braunstein, C. M. Caves, R. Jozsa, N. Linden, S. Popescu, and R. Schack, Phys. Rev. Lett. **83**, 1054 (1999).

[55] T. Byrnes, K. Wen, and Y. Yamamoto, Physical Review A **85**, 040306 (2012).

[56] H. Semenenko and T. Byrnes, Physical Review A **93**, 052302 (2016).

[57] A. N. Pyrkov and T. Byrnes, New Journal of Physics **16**, 073038 (2014).

[58] X.-H. Bao, X.-F. Xu, C.-M. Li, Z.-S. Yuan, C.-Y. Lu, and J.-W. Pan, Proceedings of the National Academy of Sciences **109**, 20347 (2012).

[59] C. Deutsch, F. Ramirez-Martinez, C. Lacroûte, F. Reinhard, T. Schneider, J.-N. Fuchs, F. Piéchon, F. Laloë, J. Reichel, and P. Rosenbusch, Physical review letters **105**, 020401 (2010).

[60] P. Treutlein, T. W. Hänsch, J. Reichel, A. Negretti, M. A. Cirone, and T. Calarco, Physical Review A **74**, 022312 (2006).

[61] E. O. Ilo-Okeke and T. Byrnes, Physical review letters **112**, 233602 (2014).

[62] A. N. Pyrkov and T. Byrnes, Physical Review A **90**, 062336 (2014).

[63] Y. Jing, M. Fadel, V. Ivannikov, and T. Byrnes, arXiv preprint arXiv:1808.10679 (2018).

[64] M. F. Riedel, P. Böhi, Y. Li, T. W. Hänsch, A. Sinatra, and P. Treutlein, Nature **464**, 1170 (2010).

[65] D. Gale, *The theory of linear economic models* (University of Chicago press, 1960).

[66] C. Navarrete-Benlloch, arXiv preprint arXiv:1504.05266 (2015).

[67] J. Johansson, P. Nation, and F. Nori, Computer Physics Communications **183**, 1760 (2012).

[68] G. Vidal and R. F. Werner, Physical Review A **65**, 032314 (2002).

[69] M. B. Plenio, Physical review letters **95**, 090503 (2005).